Phase-Imaging Ion Cyclotron Resonance data analysis for isomeric yield ratios measurement

Simone Cannarozzo[1,*], *Stephan* Pomp[1], *Andreas* Solders[1], *Ali* Al-Adili[1], *Zhihao* Gao[1], *Mattias* Lantz[1], and the IGISOL team[2]

[1]Department of Physics and Astronomy, Uppsala University, Box 516, Uppsala, 751 20, Sweden
[2]Department of Physics, Accelerator Laboratory, University of Jyvaskyla, P.O. Box 35(YFL), Jyvaskyla, 40014, Finland

Abstract. Isomeric yield ratios (IYR) are an important tool to study the angular momentum generation in nuclear fission and to investigate the possible influence on the spin of the compound nucleus formed in a fission reaction. One method to measure the IYR is to use the Phase-Imaging Ion-Cyclotron-Resonance (PI-ICR) technique. The PI-ICR is a direct ion counting technique based on the spatial separation of ions trapped in a circular motion and their projection onto a position-sensitive detector. Here the analysis routine is presented for the PI-ICR images produced to study 21 fission products formed by the 32 MeV α-induced fission of ^{232}Th at the IGISOL facility.

1 Introduction

Since its introduction in 2013 [1], the Phase-Imaging Ion-Cyclotron-Resonance (PI-ICR) has become a well-established measurement technique primarily used in nuclear mass spectrometry due to its ability to study very short-lived nuclei with high mass-resolving power.

PI-ICR is based on the combined use of a Penning trap and a position-sensitive detector, typically a micro-channel plate detector (MCP). In a Penning trap, the nuclei are trapped in a circular motion with a frequency that depends on the mass of the ion. By projecting the ion motion in the trap onto a MCP and measuring its frequency, the mass can be determined with very high accuracy.

A less common way to use PI-ICR is to measure the ratio between the production rate of two or more long-lived metastable states of a nucleus, *i.e.* the so-called isomeric yield ratio (IYR) [2–4]. The IYR can be used in a number of ways, from technological applications, *e.g.* the decay-heat calculations of spent nuclear fuel, to fundamental nuclear physics, like the study of angular momentum generation in fission [2, 5, 6]. It can also be used to test codes for both fission [7] and reaction [8] modeling.

In this work the experimental technique and the analysis process is presented for the measurement of the IYR fission products' IYR produced in the 32 MeV α-induced fission of ^{232}Th. The measurements have been performed using the IGISOL facility at the University of Jyväskylä. The measurement focused on the isomers of $^{97-100}$Y, ^{99,100,102}Nb, $^{119-125}$Cd, $^{119-127}$In, ^{129}Sn, ^{132}Sb, ^{133}Te, and ^{132,134,136}I. The IYR measurement starts with the production of the raw data, *i.e.* the PI-ICR images, followed by the data analysis to count the number of detected ions in the two isomeric states. This produces a preliminary IYR that needs to be corrected to account for the non-homogeneous detector sensitivity and the decay of ions from their production to detection, which may significantly affect the final results [4].

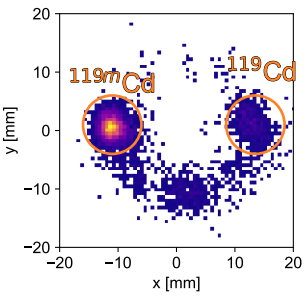

Figure 1. PI-ICR image of ^{119}Cd. The plot shows an asymmetric distribution of detected ions outside the main 2-dimensional normally distributed spots, *i.e.* the tails, and likely a third spot which might correspond to ^{119}Ag.

2 PI-ICR for IYR measurement

The IGISOL setup has already been described in detail in many publications [9] as well as its application in IYR measurements [2, 4]. Here a brief description of the main principles is presented.

A beam of charged particles is accelerated by a cyclotron and directed onto the target—in this case α-particles at 32 MeV onto ^{232}Th. The target chamber is filled with ultra-pure He gas which thermalizes the fission products (FPs) emerging from the target. After the extraction, which takes around 100 ms [10], the ions are extracted from the chamber and transported to a 55° dipole

*e-mail: simone.cannarozzo@physics.uu.se

magnet, where only ions with a selected A/q are transmitted. Before being injected in the double Penning trap system (JYFLTRAP), the continuously flowing FPs are bunched into small groups of ions. The use of two Penning traps at IGISOL allows an additional step of purification of the bunch. In the first trap, most of the contaminants are removed in order to ideally only transmit the two isomers to the second trap, where they are spatially separated and projected onto the MCP [9].

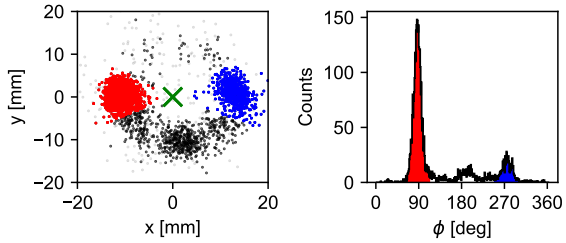

Figure 2. PI-ICR image for ^{119}Cd (left) and a polar projection of the detected ions (right). In blue and red the ions identified as high and low spin isomeric states, respectively. In black and grey, ions not considered part of the spots, and the background.

Inside a Penning trap, the ions are trapped in a rotation described by two radial eigenmotions. One of the two, the so-called reduced cyclotron motion, is characterized by a mass-dependent frequency. The difference in phase between two ions with different masses $\Delta\phi = 2\pi t\Delta\nu$ accumulated after a time t produces a space separation that is observable when the ions are projected onto the MCP (Figure 1). During the experimental campaign, the time spent by the ions in the second trap (t_{T2}) was always set in order to achieve the maximum separation between the isomeric states, *i.e.* $\Delta\phi \approx 180°$. The only exception being ^{129}Sn, where the excitation energy of the excited state is only 35 keV. The limited energy difference between the two isomers requires a long trapping time, which lowers the bunch frequency and consequently the count rate.

3 Identification method

An ideal PI-ICR image shows two 2-dimensional Gaussian-shaped clusters of detected ions corresponding to ground and excited states, separated by an angle approximately equal to 180°. The relative yields of the two nuclear states in the precision trap are therefore represented by the number of ions forming the two clusters. Two methods have been developed during previous experimental campaigns to extract IYR based on PI-ICR images produced with JYFLTRAP. One of them uses a Gaussian fit of the polar position of the detected ions [2], while the other relies on Bayesian Gaussian Mixture modeling [3, 4], to analyse more complex cases where the spots were overlapping and the MCP had a strongly non-homogeneous sensitivity. In this work, a revised version of the first method is used, as in all cases the isomeric states are well separated and the non-homogeneity of the detectors has a very limited effect.

During the experimental campaign described in this work, several nuclei resulted in images showing asymmetrical tails, as illustrated in Figure 1 and 2. While the physical interpretation of how the tails are formed is unclear, they usually correspond to 1-5% of the counts and the distortion of the spots' shape introduced is not large enough to also produce an overlap. This makes it non-trivial to define which ions should be considered to belong to a certain spot. To address this, three different methods were tested: two based on angular cuts and one on a clustering algorithm.

Angular cut with Gaussian-defined size

The polar projection of the two distributions were fitted using Gaussian distributions in order to obtain the center position θ_p and the standard deviation σ_p. The nuclei in a spot, *i.e.* in one of the two isomeric states, are defined as the ions detected at an angle between $\theta_p \pm 3\sigma_p$, as shown in Figure 2. The number of detected ions in the high-spin state C_{hs} and in the low-spin state C_{ls} are then used to calculate the IYR in the trap:

$$IYR_{exp} = \frac{C_{hs}}{C_{hs} + C_{ls}} \quad (1)$$

Angular cut with time-defined size

The standard deviation of the spots is highly influenced by the presence of either tails or close-lying contaminant peaks. Furthermore, σ_p has been shown to depend on the time the ions spend in the second trap (t_{T2}). In order for the analysis to be more robust to these distortions, C_{hs} and C_{ls} were instead calculated as the number of ions detected at an angle between $\theta_p \pm 3\sigma(t_{T2})$, where $\sigma(t_{T2})$ is the fit of the spot size as a function of t_{T2}.

Clustering (OPTICS)

A density-based clustering algorithm, called OPTICS [11], was used to assign to the same cluster datapoints that are spatially close to each other. The input parameters have been optimized in order to maximize the extension of the clusters, *i.e.* to include the tails as much as possible.

The described methods have been chosen to compare three different degrees of acceptance of the tails. Figure 3 shows that the IYRs produced by the three methods are very similar for most of the fission products. The angular cut with a time-dependent spot size is the most robust approach, where the size of the spot does not depend on the presence of the tails. Therefore, this method was ultimately used to obtain IYR_{exp}. To account for the effect of the tails, the statistical uncertainty is replaced by the standard deviation of the IYRs evaluated with the three methods when they do not match. The uncertainty is increased because it is not yet known whether the additional detected ions in the tails should be considered as part of the peak.

4 Corrections

The IYR_{exp} is the value of the yield ratio when the nuclei are detected by the MCP. To obtain the value of the actual

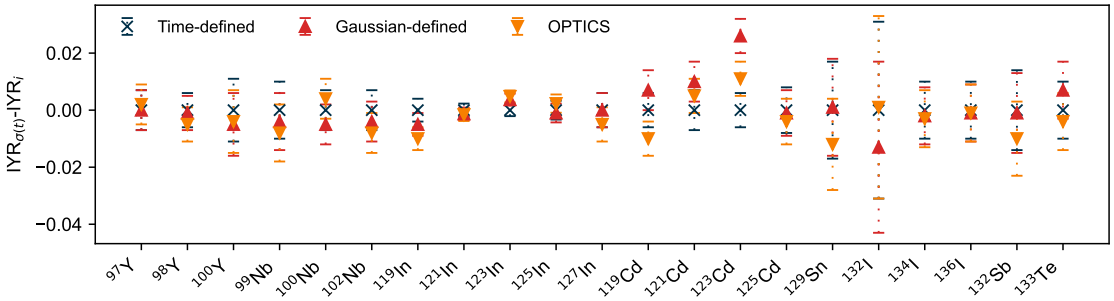

Figure 3. Comparison of IYR calculated using the three identification methods, normalized with respect to the angular cut with time-defined size ($\sigma(t)$).

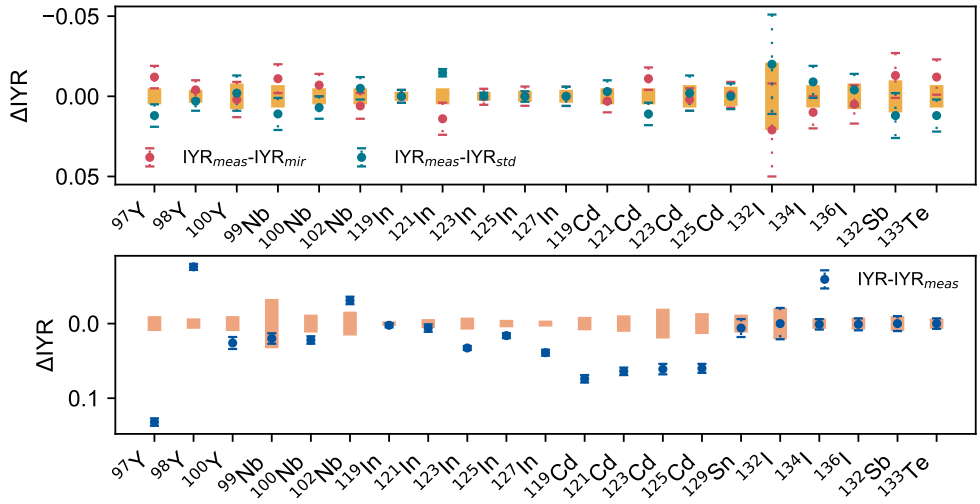

Figure 4. Top: comparison between IYRs measured based on standard and mirrored configurations with respect to the final averaged value. Bottom: Comparison between IYR$_{\text{meas}}$ and the corrected values. The yellow boxes in the two plots represent one standard deviation of IYR$_{\text{meas}}$ (top) and the final IYRs (bottom).

fission production ratio, two corrections need to be applied to account for the non-homogeneous MCP sensitivity and the decay during the transport.

The sensitivity of the MCP is not exactly homogeneous across its surface and this may significantly affect the ratio measurements [3]. An initial calibration measurement was performed, which highlighted a severe decrease in sensitivity in the upper section of the detector, *i.e.* around 0° in Figure 2. In order to mitigate this effect, the spots were always placed in the equatorial region, *i.e.* around 90° and 270°. Moreover, each measurement, except for ^{129}Sn, has been repeated in two different configurations (standard and mirrored) where the position of the two spots were exchanged. The ratio measured for both configurations is eventually merged (IYR$_{\text{meas}}$) calculating the weighted average of the two values. The effect of this correction is shown in Figure 4 (top).

The nuclei of interest and their precursors may decay during the transport process, which could significantly affect the measured ratio if their half-lives are comparable to the transport time (in the order of 0.5-1 s) [4]. The decay correction is based on a forward numerical approach where a series of balance equations are evaluated in order to simulate the transport process [12]. The model starts with an initial trial isomeric ratio after fission, followed by the transport calculation which is performed dividing each time-relevant step (target chamber, buncher, second and third trap) into 1 ms-long time intervals. For each of these intervals a balance equation is evaluated for the isomeric states of the nucleus and the two precursors, accounting for the various decays that may occur. Every nucleus may β-decay to the daughter nucleus with a characteristic half life, potentially populating the metastable excited state when present. Nuclei in the excited state may also decay to the ground state through internal transition. This process is iterated, adjusting the trial ratio until the calculated IYR matches the experimental one.

To evaluate the uncertainty, the bootstrapping procedure is applied. This simulation is repeated 10^5 times resampling all parameters, including IYR$_{\text{meas}}$, around their respective uncertainties to account for both the statistical and systematic uncertainties. Eventually the adopted IYR

is equal to the average value of the simulated IYRs, and the uncertainty to their standard deviation.

The effect of the decay correction on the ratios is shown in Figure 4. It can be seen that the correction is more relevant for the nuclei with a half-life comparable to the transport time, *i.e.* ^{97,98}Y and ^{121,123,125}Cd. Several input parameters are needed for these calculations. The half-lives are retrieved either from the Nubase2020 evaluation [13] or from the ENSDF database [14]. The independent fission yields of the nuclei are calculated using the reaction code GEF (version 2023/3.2) [15], simulating the 32 MeV alpha-particle induced fission of ^{232}Th. The branching ratios are finally estimated using the ENSDF decay schemes.

5 Conclusions

The experimental campaign of IYR measurement for the alpha-particle induced fission of ^{232}Th presented new challenges, *i.e.*, mainly, the presence of tails in the PI-ICR images. The analysis routine developed in this work presents a robust way of assessing and limiting the effect of these tails.

The mirrored measurements proved to be an effective tool in correcting the non-homogeneous sensitivity of the MCP detector.

The new model developed for the decay correction showed how this is a relevant but limited effect. Moreover, the model can be further improved by implementing additional processes, such as the oxidation or the recombination of the ions during the transport, which have been neglected in the analysis of this experiment. This model also provides an history of the ratio during the transport, opening for possible studies of the reliability of the model itself, by measuring the ratios as a function of the transport time.

The measured IYRs will be used to study the angular momentum generation in fission by comparing them to the ratios of different systems to investigate the effect of the spin and energy of the compound nucleus on the nascent fragments. They will also be used for the indirect measurement of angular momentum to further expand this investigation.

Acknowledgement

This work was supported by the Swedish Research Council (Ref. No. 2020-04238) and has received funding from the Euratom research and training program 2014-2018 under grant agreement No. 847594 (ARIEL).

References

[1] S. Eliseev, K. Blaum, M. Block, et al., Phys. Rev. Lett. **110**, 082501 (2013). 10.1103/PhysRevLett.110.082501

[2] V. Rakopoulos, M. Lantz, S. Pomp, et al., Physical Review C **99**, 014617 (2019). 10.1103/PhysRevC.99.014617

[3] Z. Gao, A. Solders, A. Al-Adili, et al. (IGISOL Collaboration), Physical Review C **108**, 054613 (2023). 10.1103/PhysRevC.108.054613

[4] Z. Gao, A. Solders, A. Al-Adili, et al., European Physical Journal A **59**, 169 (2023). 10.1140/epja/s10050-023-01080-x

[5] V. Rakopoulos, M. Lantz, A. Solders, et al., Physical Review C **98**, 024612 (2018). 10.1103/PhysRevC.98.024612

[6] Z. Gao, A. Solders, A. Al-Adili, et al., Physical Review C **109**, 064626 (2024). 10.1103/PhysRevC.109.064626

[7] A. Al-Adili, V. Rakopoulos, A. Solders, European Physical Journal A **55**, 61 (2019). 10.1140/epja/i2019-12731-5

[8] S. Cannarozzo, S. Pomp, A. Solders, et al., European Physical Journal A **59**, 295 (2023). 10.1140/epja/s10050-023-01202-5

[9] T. Eronen, V. Kolhinen, V.V. Elomaa, et al., European Physical Journal A **48**, 46 (2012). 10.1140/epja/i2012-12046-1

[10] H. Penttilä, P. Karvonen, T. Eronen, et al., The European Physical Journal A **44**, 147 (2010). 10.1140/epja/i2010-10936-8

[11] M. Ankerst, M.M. Breunig, H.P. Kriegel, J. Sander, et al., in *Proceedings of the 1999 ACM SIGMOD International Conference on Management of Data* (Association for Computing Machinery, New York, NY, USA, 1999), SIGMOD '99, pp. 49–60, ISBN 1581130848, https://doi.org/10.1145/304182.304187

[12] S. Cannarozzo, Licentiate thesis, Uppsala University, Uppsala (2023), https://urn.kb.se/resolve?urn=urn:nbn:se:uu:diva-524345

[13] F. Kondev, M. Wang, W. Huang, et al., Chinese Physics C **45**, 030001 (2021). 10.1088/1674-1137/abddae

[14] National Nuclear Data Center, From ENSDF database as of 02/21/024. version available at http://www.nndc.bnl.gov/ensarchivals (2024), [Accessed: (21/02/24)]

[15] K.H. Schmidt, B. Jurado, C. Amouroux, et al., Nuclear Data Sheets **131**, 107 (2016), special Issue on Nuclear Reaction Data. https://doi.org/10.1016/j.nds.2015.12.009